Universal experimental test for the role of free charge carriers in the thermal Casimir effect within a micrometer separation range

G. Bimonte,[1,2] G. L. Klimchitskaya,[3,4,*] and V. M. Mostepanenko[3,4,5]

[1]*Dipartimento di Fisica E. Pancini, Università di Napoli Federico II, Complesso Universitario MSA, Via Cintia, I-80126 Napoli, Italy*

[2]*INFN Sezione di Napoli, I-80126 Napoli, Italy*

[3]*Central Astronomical Observatory at Pulkovo of the Russian Academy of Sciences, Saint Petersburg 196140, Russia*

[4]*Institute of Physics, Nanotechnology and Telecommunications, Peter the Great Saint Petersburg Polytechnic University, Saint Petersburg 195251, Russia*

[5]*Kazan Federal University, Kazan 420008, Russia*

(Received 10 April 2017; published 26 May 2017)

We propose a universal experiment to measure the differential Casimir force between a Au-coated sphere and two halves of a structured plate covered with a P-doped Si overlayer. The concentration of free charge carriers in the overlayer is chosen slightly below the critical one, for which the phase transition from dielectric to metal occurs. One half of the structured plate is insulating, while the second half is made of gold. For the former we consider two structures, one consisting of bulk high-resistivity Si and the other of a layer of SiO_2 followed by bulk high-resistivity Si. The differential Casimir force is computed within the Lifshitz theory using four approaches that have been proposed in the literature to account for the role of free charge carriers in metallic and dielectric materials interacting with quantum fluctuations. According to these approaches, Au at low frequencies is described by either the Drude or the plasma model, whereas the free charge carriers in dielectric materials at room temperature are either taken into account or disregarded. It is shown that the values of differential Casimir forces, computed in the micrometer separation range using these four approaches, are widely distinct from each other and can be easily discriminated experimentally. It is shown that for all approaches the thermal component of the differential Casimir force is sufficiently large for direct observation. The possible errors and uncertainties in the proposed experiment are estimated and its importance for the theory of quantum fluctuations is discussed.

DOI: 10.1103/PhysRevA.95.052508

I. INTRODUCTION

During the last two decades the Casimir force [1] acting between two closely spaced uncharged material surfaces has attracted much experimental and theoretical attention due to the diverse roles it plays in both fundamental and applied physics (see monograph [2] and reviews [3–5]). The Casimir effect is an entirely quantum and (at separations between surfaces exceeding 2 or 3 nm) relativistic phenomenon. In the nonrelativistic region the Casimir force is commonly known as the van der Waals force [6]. The Casimir effect is caused by zero-point and thermal fluctuations of the electromagnetic field. Although Casimir [1] calculated the force acting between two ideal metal planes, Lifshitz [7] developed a general theory of van der Waals and Casimir forces between two parallel material plates described by the respective frequency-dependent dielectric permittivities. In recent years this theory has been generalized to the case of arbitrarily shaped interacting bodies [5].

In 2000 it was shown that the Lifshitz theory leads to widely different predictions for the thermal Casimir force between metallic test bodies depending on whether the low-frequency dielectric response of metals is described by the lossy Drude [8] or by the lossless plasma [9] model. Later it was demonstrated that if the Drude model is used, the Casimir entropy calculated within the Lifshitz theory does not satisfy the third law of thermodynamics (the Nernst heat theorem) for either nonmagnetic [10–13] or magnetic [14] metals with perfect crystal lattices. If instead the plasma model is used, the Lifshitz theory is found to be in perfect agreement with the Nernst theorem [10–14]. By contrast, in the limiting case of large separations between metallic plates, for which classical statistical physics should be applicable, a first-principle computation based on a microscopic model was shown in Ref. [15] to reproduce the Casimir force predicted by the Lifshitz theory combined with the Drude model. The Drude model was shown to satisfy the Bohr–van Leeuwen theorem of classical statistical physics, which is, however, violated if the plasma model is used to calculate the Casimir force at large separations [16]. It was shown also that the difference in theoretical predictions of the Drude versus the plasma models could be attributed to the magnetic interaction among fluctuating Foucault currents [17–19].

In two series of precise experiments on measuring the Casimir interaction between metals by means of a micromechanical oscillator [20–23] and an atomic force microscope [24–26], theoretical predictions of the Lifshitz theory using the Drude model dielectric response at low frequencies have been excluded by the measurement data at a confidence level of up to 99%. The theoretical predictions obtained using the plasma model turned out to be in agreement with the data at a 90% confidence level [27]. All these experiments were performed at separations below 1 μm, where the difference between the theoretical predictions using the Drude and those using the plasma models does not exceed a few percent. The only experiment performed at separations up to 7.3 μm was interpreted to be in agreement

*g_klimchitskaya@mail.ru

with theoretical predictions of the Lifshitz theory combined with the Drude model [28]. It was noted, however, that in Ref. [28] the Casimir force was extracted by means of a fitting procedure from a measured force up to an order of magnitude larger, supposedly originating from electrostatic patches and influenced by imperfections, which are unavoidably present on the surfaces of lenses with centimeter-size radii [29,30]. Thus, the majority of experiments on measuring the Casimir force do confirm the lossless plasma model. Since the relaxation of free electrons in metals at low frequencies is a much studied fact, this situation is regarded in the literature as the Casimir puzzle.

The Casimir force acting on dielectric bodies also presents a puzzle. The problem is that the measurement data from all precise experiments with dielectric surfaces are in agreement with theoretical predictions of the Lifshitz theory only provided that the contribution of free charge carriers in the dielectric response (dc conductivity) is omitted in computations [31–34]. If the dc conductivity of dielectric bodies is taken into account, the theoretical predictions of the Lifshitz theory are excluded by the measurement data [31–35]. Similarly to the role of relaxation of free charge carriers in metallic bodies, the influence of the dc conductivity in the Casimir force on dielectric bodies is limited to just a few percent of the measured signal. Theoretically it was proven that the Lifshitz theory with the dc conductivity of dielectric materials included violates the Nernst heat theorem, while agreement with this theorem is restored when the dc conductivity is omitted [36–39]. This makes us again disregard a real physical phenomenon (here, the conductivity of a dielectric material at nonzero temperature) to achieve agreement with both experimental data and the third law of thermodynamics.

It is noteworthy that the impact of both relaxation phenomena in metals and of the dc conductivity in dielectrics on the Casimir force at separations below 1 μm is always relatively small. Then one may hope that by a proper account of some background effects due to, e.g., electrostatic patches [40] or surface roughness [3,41], one could bring the predictions of the literally understood Lifshitz theory in agreement with the data. To investigate this possibility, Ref. [42] proposed measuring the Casimir force between two aligned sinusoidally corrugated Ni surfaces, one of which is coated with a thin opaque Au layer having a flat surface. According to the results obtained, the phase-dependent modulation of the Casimir force for submicron separations, predicted by the Drude model, is several orders of magnitude larger than that predicted by the plasma model. An experiment based on this principle [43] has measured the differential force between Au- or Ni-coated spheres and Au and Ni sectors of a structured disk covered with an Au overlayer at separations of a few hundred nanometers. The measurement data unequivocally ruled out the Drude model and were found to be in good agreement with those for the plasma model [43]. This experiment is immune to electrostatic forces caused by patch potentials similarly to isoelectronic differential force measurements searching for Yukawa-type corrections to Newton's gravitational law [44,45]. It is interesting to point out that the Casimir free energies and pressures of thin metallic films computed using the Drude and plasma models have also been found to differ by up to a factor of several thousand [46–48]. It is found again that the Nernst heat theorem is violated if the Drude model is used in computations [49].

In view of the above considerations it would clearly be desirable to perform an experimental test on the role of free charge carriers in the Casimir force in the micrometer separation range where thermal effects are most pronounced. Differential force measurements of this sort have been proposed in Refs. [50] and [51] for both nonmagnetic and magnetic metallic test bodies. The setup considered in Refs. [50] and [51] involved a structured plate, one half of which was made of a metal (Au or Ni) and the other half of high-resistivity Si. The structured plate was covered with a plane-parallel overlayer made of a B-doped Si plate in the metallic state with a thickness of 100 nm. This setup allows for a measurable differential force between a metal-coated sphere and the two halves of a sample which is of a quite different magnitude depending on whether the metal is described by the Drude or the plasma model. The test in Refs. [50] and [51] is not sensitive, however, to the dc conductivity of high-resistivity Si.

In this paper, we propose a universal test for the role of free charge carriers in the Casimir force in the micrometer range of separations. It follows the main idea in Refs. [50] and [51], i.e., it suggests measuring the differential Casimir force between a Au-coated sphere and the high-resistivity Si and Au halves of a structured plate. The main difference is, however, that we now consider a semitransparent overlayer made of P-doped Si with a concentration of free charge carriers which is only slightly lower than the critical concentration at which the dielectric-to-metal phase transition occurs. This means that the overlayer used is in a dielectric state, although it preserves all the experimental advantages of having a rather high electronic conductivity.

We calculate the differential Casimir force in a configuration including both metallic and dielectric materials using the following four theoretical approaches: in the first one Au at low frequencies is described by the plasma model and the conductivity of Si is disregarded; in the second approach Au at low frequencies is described by the plasma model but the conductivity of Si is taken into account; in the third one Au at low frequencies is described by the Drude model but the conductivity of Si is disregarded; finally, in the fourth approach the low-frequency dielectric response of Au is described by the Drude model and the conductivity of Si is taken into account. We compute the differential Casimir force using these four approaches and show that in all of them the obtained results are widely different in the micrometer separation range and can be easily discriminated using the already available experimental setup. It is shown that the proposed experiment allows for precise measurement of the thermal effect in the Casimir force. We also propose a modified structure of the plate by adding a layer of SiO_2, which offers some advantages in the process of plate preparation and further increases the relative differences between the theoretical predictions made by the four approaches. Computations of the differential Casimir forces are performed using the tabulated optical data on all involved materials over the frequency ranges for which they are available. The estimation of both theoretical and experimental errors and uncertainties in the proposed experiment demonstrates its feasibility.

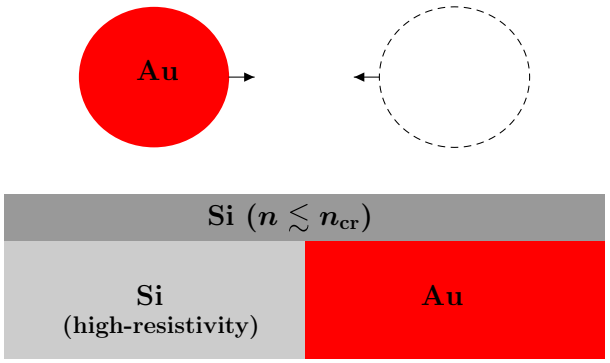

FIG. 1. Experimental configuration of a Au sphere moving back and forth above a structured plate covered with a P-doped Si overlayer in the dielectric state. The measured quantity is the differential Casimir force $F_{\rm diff}$ between the Au sphere and the two halves of the plate when the sphere bottom is far away from their boundaries. The figure displays the two extreme positions of the sphere during its motion. The size of the sphere is not shown to scale.

The structure of the paper is as follows. In Sec. II the principle scheme of the proposed experiment is outlined and the general formalism is presented. Section III reports the results of numerical computations of the differential Casimir force within the four theoretical approaches. Section IV presents the modified experimental scheme and more detailed computational results for the differential force. In Sec. V all errors and uncertainties are estimated. In Sec. VI the reader will find our discussion and conclusions.

II. PRINCIPAL EXPERIMENTAL SCHEME AND GENERAL FORMALISM

We consider the configuration of a Au-coated sapphire sphere with radius $R = 150\ \mu$m in vacuum, at a separation a from a structured plate at room temperature $T = 300$ K. The thickness of the Au coating is assumed to exceed 100 nm, in such a way that it is legitimate to consider the sphere to be made entirely of gold, for the sake of computing the Casimir force. The structured plate consists of an overlayer made of P-doped Si of thickness $d = 100$ nm covering two sections, one of which is made of high-resistivity Si and the other of Au (see Fig. 1). The thickness of both sections is large enough to consider them as two semispaces. We consider an overlayer with a rather high electronic conductivity which corresponds to the density of free charge carriers $n = 3.5 \times 10^{18}$ cm^{-3}. This density is, however, slightly lower than the critical density $n_{\rm cr} = 3.84 \times 10^{18}$ cm^{-3} at which the dielectric-to-metal phase transition occurs [52]. Thus, both the overlayer and the underlying left section of the plate are made of dielectric materials, although with quite different free charge carrier densities.

We denote the materials of the sphere, of the overlayer, and of the left section of the plate 1, 2, and 3, respectively. Then the material of the right section of the plate is also denoted 1. We denote the vacuum gap material 0. The respective dielectric permittivities at the pure imaginary Matsubara frequencies are

$$\varepsilon_k(i\xi_l) = \varepsilon_k\left(i\frac{c\zeta_l}{2a}\right) \equiv \varepsilon_{k,l}. \tag{1}$$

Here, $k = 0, 1, 2, 3$, $\xi_l = 2\pi k_B T l/\hbar$ with $l = 0, 1, 2, \ldots$ and k_B being the Boltzmann constant are the Matsubara frequencies, and ζ_l are the dimensionless Matsubara frequencies. For a vacuum gap we have $\varepsilon_{0,l} = 1$.

In the proposed experiment the sphere moves back and forth at a sufficiently high frequency at some fixed separation a from the plate. In this case not the Casimir forces $F_{\rm Si}(a,T)$ and $F_{\rm Au}(a,T)$ among the Au sphere and the left and right sections of the plate but only the difference $F_{\rm diff}(a,T)$ between them is measured [43–45]:

$$F_{\rm diff}(a,T) = F_{\rm Si}(a,T) - F_{\rm Au}(a,T). \tag{2}$$

This measurement should be repeated at different separations. Note that $F_{\rm Si}(a,T)$ and $F_{\rm Au}(a,T)$ are the forces acting when the sphere bottom is above some points deep in the left and right halves of the plate, respectively. Because of this, one can neglect the effect of the sharp boundary between the left and the right halves of the plate and consider each of them to be infinitely large [51].

Using the proximity force approximation [2], which was recently shown to be sufficiently exact under the condition $a \ll R$ [53–55], and the Lifshitz formula [2,7], the differential force, (2), can be calculated by the equation

$$F_{\rm diff}(a,T) = \frac{k_B T R}{4a^2}{\sum_{l=0}^{\infty}}' \int_{\zeta_l}^{\infty} y\,dy \times \sum_{\alpha} \ln\frac{1 - r_\alpha^{(0,1)}(i\zeta_l,y)R_\alpha^{(0,2,3)}(i\zeta_l,y)e^{-y}}{1 - r_\alpha^{(0,1)}(i\zeta_l,y)R_\alpha^{(0,2,1)}(i\zeta_l,y)e^{-y}}, \tag{3}$$

where the prime on the summation sign denotes that the $l = 0$ term is taken with weight 1/2. Here, y is the dimensionless variable connected with the projection of the wave vector onto the plane of the plate, $\boldsymbol{k}_\perp$, by

$$y = 2a\sqrt{\boldsymbol{k}_\perp^2 + \frac{\xi_l^2}{c^2}}. \tag{4}$$

The summation in α is made over the two independent polarizations of the electromagnetic field, transverse magnetic ($\alpha = {\rm TM}$) and transverse electric ($\alpha = {\rm TE}$). The reflection coefficients on the structured plate covered with the overlayer are expressed as

$$R_\alpha^{(0,2,j)}(i\zeta_l,y) = \frac{r_\alpha^{(0,2)}(i\zeta_l,y) + r_\alpha^{(2,j)}(i\zeta_l,y)e^{-d\sqrt{y^2+(\varepsilon_{2,l}-1)\zeta_l^2}/a}}{1 + r_\alpha^{(0,2)}(i\zeta_l,y)r_\alpha^{(2,j)}(i\zeta_l,y)e^{-d\sqrt{y^2+(\varepsilon_{2,l}-1)\zeta_l^2}/a}}, \tag{5}$$

where $j = 1, 3$. Finally, the reflection coefficients on the boundary surfaces between two different materials are given by the familiar Fresnel formulas taken at the imaginary Matsubara frequencies:

$$r_{\rm TM}^{(k,j)}(i\zeta_l,y) = \frac{\varepsilon_{j,l}\sqrt{y^2+(\varepsilon_{k,l}-1)\zeta_l^2} - \varepsilon_{k,l}\sqrt{y^2+(\varepsilon_{j,l}-1)\zeta_l^2}}{\varepsilon_{j,l}\sqrt{y^2+(\varepsilon_{k,l}-1)\zeta_l^2} + \varepsilon_{k,l}\sqrt{y^2+(\varepsilon_{j,l}-1)\zeta_l^2}},$$

$$r_{\rm TE}^{(k,j)}(i\zeta_l,y) = \frac{\sqrt{y^2+(\varepsilon_{k,l}-1)\zeta_l^2}-\sqrt{y^2+(\varepsilon_{j,l}-1)\zeta_l^2}}{\sqrt{y^2+(\varepsilon_{k,l}-1)\zeta_l^2}+\sqrt{y^2+(\varepsilon_{j,l}-1)\zeta_l^2}}, \tag{6}$$

where $(k,j) = (0,1)$, $(0,2)$, $(2,1)$, and $(2,3)$.

The contribution to Eq. (3) at zero Matsubara frequency requires special attention because the problems discussed in Sec. I are connected with different treatments of this contribution. The point is that the optical data for the complex index of refraction of all materials are available only for sufficiently high frequencies. Therefore, at low frequencies the available data should be supplemented with some theoretical model. Taking into account the relaxation properties of electrons in metals, the dielectric permittivities of our material 1 (Au) at the Matsubara frequencies can be represented in the form

$$\varepsilon_{1,l}^{D} = \frac{\tilde{\omega}_{p,1}^2}{\zeta_l(\zeta_l+\tilde{\gamma}_1)} + \varepsilon_{1,l}^{\rm cor}. \tag{7}$$

Here, $\tilde{\omega}_{p,1}$ and $\tilde{\gamma}_1$ are, respectively, the dimensionless plasma frequency and relaxation parameter of Au, connected with the dimensional ones by

$$\tilde{\omega}_{p,1} = \frac{2a\omega_{p,1}}{c}, \quad \tilde{\gamma}_1 = \frac{2a\gamma_1}{c}, \tag{8}$$

and $\varepsilon_{1,l}^{\rm cor}$ is a contribution of the core (bound) electrons to the dielectric permittivity determined by the optical data. The upper index D is used to emphasize that the permittivity, (7), has the Drude form. Note that the relaxation parameter $\tilde{\gamma}_1$ depends on the temperature and goes to 0 with vanishing T by a power law. For metals with disregarded relaxation properties of free electrons the dielectric permittivity takes the plasma form

$$\varepsilon_{1,l}^{p} = \frac{\tilde{\omega}_{p,1}^2}{\zeta_l^2} + \varepsilon_{1,l}^{\rm cor}. \tag{9}$$

The plasma model is usually used in the region of infrared optics where $\gamma_1 \ll \xi_l$.

For dielectric materials ($k = 2, 3$) with free charge carriers taken into account the dielectric permittivity at the Matsubara frequencies takes the form

$$\varepsilon_{k,l} = \frac{4\pi\tilde{\sigma}_{k,l}}{\zeta_l} + \varepsilon_{k,l}^{\rm cor}, \tag{10}$$

where the dimensionless conductivity $\tilde{\sigma}_{k,l}$ is connected with the dimensional one by

$$\tilde{\sigma}_{k,l} = \frac{2a\sigma_{k,l}}{c}. \tag{11}$$

The conductivity of dielectrics is temperature dependent. It vanishes exponentially rapidly when T goes to 0. At room temperature it is customary to represent the frequency dependence of $\tilde{\sigma}_{k,l}$ in terms of conventional Drude parameters, i.e., as

$$\tilde{\sigma}_{k,l} = \frac{\tilde{\omega}_{p,k}^2}{4\pi(\zeta_l+\tilde{\gamma}_k)}. \tag{12}$$

If the free charge carriers in dielectric materials are disregarded, it holds that

$$\varepsilon_{k,l} = \varepsilon_{k,l}^{\rm cor}, \quad k = 2, 3. \tag{13}$$

For our dielectric materials with $k = 2$ (P-doped Si) and $k = 3$ (high-resistivity Si)

$$\varepsilon_{2,l}^{\rm cor} = \varepsilon_{3,l}^{\rm cor}, \tag{14}$$

although $\tilde{\sigma}_{2,l}$ and $\tilde{\sigma}_{3,l}$ are significantly different. Note also that for both metals and dielectrics $\varepsilon_{k,l}^{\rm cor} \to 1$ when $\zeta_l \to \infty$.

First, we assume that the free charge carriers in both dielectric materials (i.e., in the overlayer made of doped Si and in the plate section of high-resistivity Si) are disregarded. Then, at $l = 0$ Eqs. (13) and (14) hold. In this case, from the first line of Eq. (6) one obtains $r_{\rm TM}^{(2,3)}(0,y) = 0$ and from Eq. (5) we have

$$R_{\rm TM}^{(0,2,3)}(0,y) = r_{\rm TM,0}^{(0,2)} = \frac{\varepsilon_{2,0}^{\rm cor}-1}{\varepsilon_{2,0}^{\rm cor}+1}. \tag{15}$$

Now, from the first line of Eq. (6), one can see that $r_{\rm TM}^{(2,1)}(0,y) = 1$ independently of whether Au is described by the Drude model of Eq. (7) or by the plasma model of Eq. (9). Then Eq. (5) leads to

$$R_{\rm TM}^{(0,2,1)}(0,y) = \frac{r_{\rm TM,0}^{(0,2)}+e^{-dy/a}}{1+r_{\rm TM,0}^{(0,2)}e^{-dy/a}}, \tag{16}$$

where $r_{\rm TM,0}^{(0,2)}$ is given by Eq. (15).

From the second line of Eq. (6) we have

$$r_{\rm TE}^{(0,2)}(0,y) = r_{\rm TE}^{(2,3)}(0,y) = 0. \tag{17}$$

Then, from Eq. (5) one obtains

$$R_{\rm TE}^{(0,2,3)}(0,y) = 0. \tag{18}$$

As for the reflection coefficient $R_{\rm TE}^{(0,2,1)}(0,y)$, its value depends on whether Au is described by the Drude or the plasma model. If the Drude model, (7), is used, the second line of Eq. (6) leads to $r_{{\rm TE},D}^{(2,1)}(0,y) = 0$ and Eq. (5) results in

$$R_{{\rm TE},D}^{(0,2,1)}(0,y) = 0, \tag{19}$$

similarly to Eq. (18). If, however, the plasma model, (9), is used for Au, the second line of Eq. (6) leads to

$$r_{{\rm TE},p}^{(2,1)}(0,y) = \frac{y-\sqrt{y^2+\tilde{\omega}_{p,1}^2}}{y+\sqrt{y^2+\tilde{\omega}_{p,1}^2}}, \tag{20}$$

and from Eq. (5) one obtains

$$R_{{\rm TE},p}^{(0,2,1)}(0,y) = \frac{y-\sqrt{y^2+\tilde{\omega}_{p,1}^2}}{y+\sqrt{y^2+\tilde{\omega}_{p,1}^2}}\,e^{-dy/a}. \tag{21}$$

Next, we make the alternative assumption that the free charge carriers in dielectric materials are taken into account by Eq. (10). In this case $r_{\rm TM}^{(0,2)}(0,y) = 1$ and from Eq. (5) we have

$$R_{\rm TM}^{(0,2,3)}(0,y) = R_{\rm TM}^{(0,2,1)}(0,y) = 1. \tag{22}$$

Note that the latter equation is valid irrespective of whether Au is described by the Drude or the plasma models. For the TE mode Eq. (17) is still valid, leading to

$$R_{\rm TE}^{(0,2,3)}(0,y)=0. \tag{23}$$

The value of the coefficient $R_{\rm TE}^{(0,2,1)}(0,y)$ depends on the model used for a description of Au. If the Drude model is used,

$$r_{{\rm TE},D}^{(2,1)}(0,y)=R_{{\rm TE},D}^{(0,2,1)}(0,y)=0. \tag{24}$$

If, however, Au is described by the plasma model, one returns to Eqs. (20) and (21), which preserve their validity when the free charge carriers in dielectric materials are taken into account.

From the above one can see that at zero Matsubara frequency the coinciding reflection coefficients $R_{\rm TE}^{(0,2,j)}$ with $j=1,3$ are obtained in cases where the free charge carriers of the dielectric materials 2 and 3 are either disregarded or taken into account. In each case, however, the results for $R_{\rm TE}^{(0,2,1)}$ depend on the model used for a description of Au. Just the opposite situation holds for the coefficients $R_{\rm TM}^{(0,2,j)}$ calculated at $\zeta_0=0$. Here, the results do not depend on the model of a metal but differ depending on whether or not the free charge carriers of dielectric materials are taken into account.

III. DISCRIMINATION BETWEEN DIFFERENT THEORETICAL APPROACHES

Now we perform numerical computations of the differential Casimir force, (2), in the configuration in Sec. II by using Eqs. (3)–(5) and the explicit expressions for the reflection coefficients at zero Matsubara frequency provided in Eqs. (15), (16), (18), (19), and (21)–(24), obtained in the framework of different theoretical approaches. The dielectric permittivities $\varepsilon_{k,l}^{\rm cor}$ of Au and Si at the Matsubara frequencies were obtained using the tabulated optical data for the complex index of refraction [56,57] and the Kramers-Kronig relation following Refs. [2] and [3]. For Au the values of the plasma frequency $\omega_{p,1}\approx 9$ eV $=1.37\times10^{16}$ rad/s and the relaxation parameter $\gamma_1\approx 35$ meV $=5.3\times10^{13}$ rad/s have been used.

For P-doped Si the chosen concentration of free electrons ($n=3.5\times10^{18}$ cm^{-3}) corresponds to the plasma frequency

$$\omega_{p,2}=e\sqrt{\frac{4\pi n}{m^*}}\approx 2.1\times10^{14}\ {\rm rad/s}, \tag{25}$$

where the effective electron mass is $m^*=0.26m_e$. The chosen value of n corresponds also to the resistivity $\rho_2=(1.4\pm0.1)\times10^{-2}\ \Omega\,{\rm cm}$ [58], i.e., $\rho_2\approx1.55\times10^{-14}$ s and the conductivity $\sigma_2\approx0.64\times10^{14}$ s^{-1}. If one models the conductivity of P-doped Si at a fixed $T=300$ K by means of the Drude model, this value of conductivity leads to the following relaxation parameter [59]:

$$\gamma_2=\frac{\omega_{p,2}^2}{4\pi\sigma_2}=\frac{1}{4\pi}\rho_2\omega_{p,2}^2\approx5.5\times10^{13}\ {\rm rad/s}. \tag{26}$$

Now we consider material 3, i.e., high-resistivity Si, whose conductivity is lower than that of our P-doped Si by about five orders of magnitude. If the free charge carriers in Si are disregarded, materials 2 and 3 become identical and their common dielectric permittivity is given by $\varepsilon_{2,l}^{\rm cor}$. Note that for Si $\varepsilon_{2,0}^{\rm cor}\approx11.67$. The inclusion of free charge carriers for high-resistivity Si affects the dielectric permittivity only at the zero Matsubara frequency and results in nonzero dc conductivity. Now we take into account that according to Eqs. (18) and (23) the reflection coefficient $R_{\rm TE}^{(0,2,3)}(0,y)$ takes the same value irrespective of whether one includes or neglects the contribution to the permittivity of free charge carriers in Si. On the contrary, the value of the coefficient $R_{\rm TM}^{(0,2,3)}(0,y)$ does depend on whether or not one includes the contribution of free charge carriers in the P-doped Si overlayer [see Eqs. (15) and (22)]. However, even in this case it does not depend on the conductivity properties of high-resistivity Si.

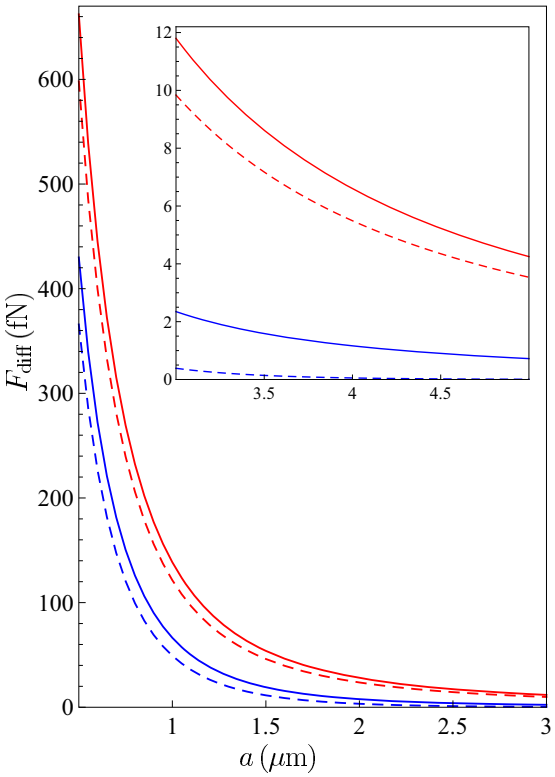

FIG. 2. Differential Casimir forces computed at $T=300$ K for the configuration in Fig. 1 using the plasma model for Au with free charge carriers in dielectric materials disregarded and taken into account [top (red) pair of solid and dashed lines, respectively] and using the Drude model for Au with free charge carriers in dielectrics disregarded and included [bottom (blue) pair of solid and dashed lines, respectively] are shown as functions of the separation. Inset: Region of larger distances.

The results of the computations for the differential Casimir force, (2), at $T=300$ K are presented in Fig. 2 as functions of the separation in the range from 0.5 to 3 μm and, on an enlarged scale, in the inset in the range from 3 to 5 μm. The top pair of lines (solid and dashed) is computed using the plasma model, (9), for Au. The free charge carriers in both the P-doped and the high-resistivity Si are either disregarded according to Eq. (13) (solid line) or taken into account according to Eq. (10) (dashed line). In a similar way, the bottom pair of solid and dashed lines is computed using the Drude model, (7), for Au. Here, the solid line is again computed by disregarding the free

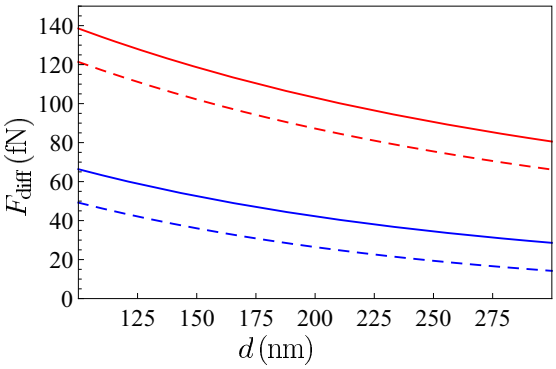

FIG. 3. Differential Casimir forces computed at $T = 300$ K in the configuration in Fig. 1 using the plasma model for Au with free charge carriers in dielectric materials disregarded and taken into account [top (red) pair of solid and dashed lines, respectively] and using the Drude model for Au with free charge carriers in dielectrics disregarded and included [bottom (blue) pair of solid and dashed lines, respectively] are shown as functions of the overlayer thickness at $a = 1$ μm.

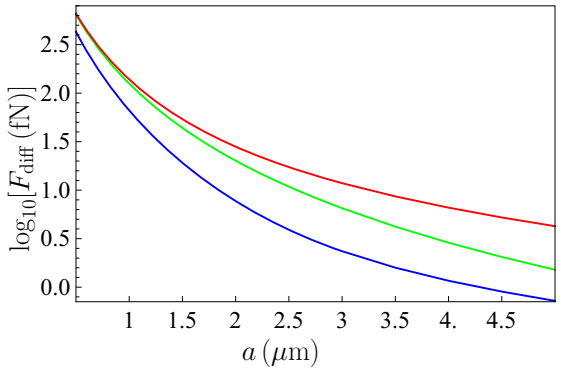

FIG. 4. Logarithm of the differential Casimir forces computed at $T = 300$ K using the plasma and the Drude models for Au with free charge carriers in dielectric materials disregarded is shown as functions of the separation by the top (red) and bottom (blue) lines, respectively. The middle (green) line shows common computational results for the differential Casimir force at zero temperature.

charge carriers in dielectric materials and the dashed line takes these charge carriers into account.

As shown in Fig. 2, the four theoretical approaches discussed in Sec. I lead to widely different predictions for the differential Casimir force. They can be easily discriminated experimentally keeping in mind that the sensitivity of difference force measurements of this type is equal to 1 fN [43] or even a fraction of 1 fN [45]. Thus, for $a = 1$ μm use of the plasma model for Au results in $F^{p}_{\rm diff} \approx 138.54$ fN and $F^{p,{\rm dc}}_{\rm diff} \approx 120.66$ fN with free charge carriers disregarded and included, respectively, in both the P-doped Si overlayer and the high-resistivity Si (top pair of lines). If Au is described by the Drude model and the free charge carriers are either disregarded or included, one has $F^{D}_{\rm diff} \approx 66.37$ fN or $F^{D,{\rm dc}}_{\rm diff} \approx 48.50$ fN, respectively (bottom pair of lines). It is shown that the four theoretical predictions are approximately 18, 54, and 18 fN apart, i.e., the force intervals between them far exceed the experimental sensitivity. Even for $a = 2$ μm we have $F^{p}_{\rm diff} \approx 28.07$ fN and $F^{p,{\rm dc}}_{\rm diff} \approx 23.63$ fN with free charge carriers in Si materials disregarded and taken into account, respectively, and $F^{D}_{\rm diff} \approx 7.71$ fN and $F^{D,{\rm dc}}_{\rm diff} \approx 3.26$ fN under the same assumptions about the free charge carriers. Here, the theoretical predictions are approximately 5, 16, and 4 fN apart, i.e., again can be experimentally discriminated (see Sec. V for additional information about errors and uncertainties in this experiment).

In the above computations, a P-doped Si overlayer of $d = 100$ nm thickness has been used. It is interesting to determine the dependence of $F_{\rm diff}$ on d. In Fig. 3 the computational results for the differential Casimir force at $a = 1$ μm, $T = 300$ K are presented as a function of the overlayer thickness using the four theoretical approaches described above (the top pair of solid and dashed lines is computed using the plasma model for Au with free charge carriers in Si disregarded and included, respectively; the bottom pair of solid and dashed lines is computed using the Drude model with free charge carriers in Si either disregarded or included). As shown in Fig. 3, the differential Casimir force decreases monotonously with increasing d, while the discrepancies between the theoretical predictions of the different models are almost independent of the thickness. This feature of the force makes a thicker overlayer (for instance, $d = 200$ nm; see Sec. IV) preferable because in this case the relative error in the determination of d becomes negligibly small and therefore it does not influence the value of $F_{\rm diff}$. A more detailed analysis of theoretical errors is given in Sec. V.

Now we show that the proposed experiment not only allows for an easy discrimination between the four theoretical approaches described above, but can be used to measure the thermal effect on $F_{\rm diff}$ as well. First, we illustrate this statement for the case of Au described by either the Drude or the plasma model with free charge carriers in Si disregarded. In Fig. 4 the bottom (Drude model) and the top (plasma model) solid lines are reproduced from Fig. 2 using a logarithmic scale along the axis of $F_{\rm diff}$. The middle line in Fig. 4 shows the computational results for $F_{\rm diff}$ obtained at $T = 0$ K. For perfect crystal lattices the relaxation parameter $\gamma(T = 0) = 0$, so that the theoretical results obtained using the Drude and plasma models coincide. For real metals, however, there is some small residual relaxation $\gamma_{\rm res}(T = 0) \neq 0$. We have used $\gamma_{\rm res,1} = 1.2 \times 10^{-6}$ eV for Au and obtained the same middle line in Fig. 4 as given by the plasma model. Numerically, the computational results turned out to be very close. For example, at $a = 0.5$, 1.0 and 1.5 μm the differential Casimir forces computed at $T = 0$ using the Drude and the plasma models are equal to 643.11 and 643.86, 124.96 and 125.19, and 43.64 and 43.76 fN, respectively.

As shown in Fig. 4, at separations $a = 0.5$, 1.0, 1.5, 2.0, and 2.5 μm the thermal correction in $F_{\rm diff}$,

$$\Delta_T F_{\rm diff}(a,T) = F_{\rm diff}(a,T) - F_{\rm diff}(a,0), \qquad (27)$$

computed using the Drude model (i.e., the difference between the bottom and the middle lines) is equal to -213.28, -58.59, -24.50, -12.34, and -6.5 fN, respectively. Note that the quantity $F_{\rm diff}(a,0)$ in Eq. (27) is computed by the zero-temperature Lifshitz formula [2,7], where one makes an integration over the continuous frequency ζ instead of a summation over the discrete Matsubara frequencies ζ_l and uses the

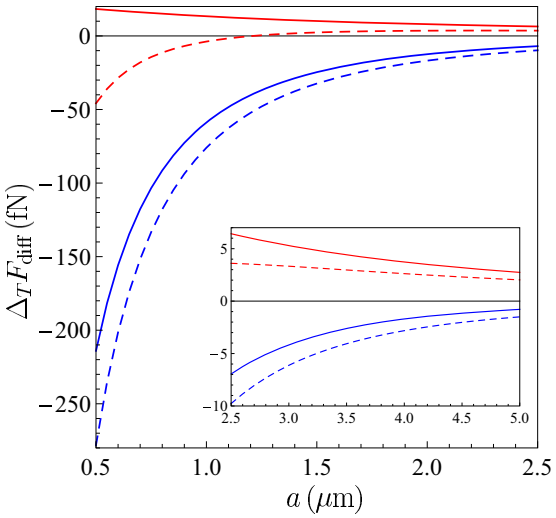

FIG. 5. Thermal corrections to the differential Casimir forces at $T = 300$ K computed using the plasma model for Au with free charge carriers in dielectric materials disregarded and taken into account [top (red) pair of solid and dashed lines, respectively] and using the Drude model for Au with free charge carriers in dielectrics disregarded and included [bottom (blue) pair of solid and dashed lines, respectively] are shown as functions of the separation. Inset: Region of larger distances.

zero-temperature values of all involved dielectric permittivities. The thermal correction in $F_{\rm diff}$ computed using the plasma model (i.e., the difference between the top and the middle lines) is equal to 18.3, 13.35, 10.11, 7.95, and 6.42 fN. In all these cases the magnitudes of the thermal effect are far greater than the experimental sensitivity.

In Fig. 5 we present the computational results for the thermal correction, (27), as functions of separation at $T = 300$ K using the four theoretical approaches described above. The top pair of solid and dashed lines is computed using the plasma model for Au with free charge carriers of dielectrics omitted and included, respectively. The bottom pair of solid and dashed lines is also computed by disregarding and including the free charge carriers in dielectrics, but describing Au with the Drude model. The thermal corrections presented by the top and bottom solid lines (the plasma and Drude models for Au with omitted charge carriers in dielectrics) have been discussed above on the basis of Fig. 4. The thermal correction shown by the bottom dashed line (the Drude model for Au with free charge carriers in dielectrics included) can be easily observed over the separation range from 0.5 to 2.5 μm and discriminated from the bottom solid line. As for the thermal correction shown by the top dashed line (the plasma model for Au with free charge carriers in dielectrics included), it can be observed within the separation range from 0.5 to 0.9 μm.

It is instructive to separate the thermal correction to the differential force, (27), into two parts:

$$\Delta_T F_{\rm diff}(a,T) = \Delta_T^{(1)} F_{\rm diff}(a,T) + \Delta_T^{(2)} F_{\rm diff}(a,T). \tag{28}$$

Here, we have introduced the notations

$$\begin{aligned} \Delta_T^{(1)} F_{\rm diff}(a,T) &= \tilde{F}_{\rm diff}(a,T) - F_{\rm diff}(a,0), \\ \Delta_T^{(2)} F_{\rm diff}(a,T) &= F_{\rm diff}(a,T) - \tilde{F}_{\rm diff}(a,T), \end{aligned} \tag{29}$$

where $\tilde{F}_{\rm diff}(a,T)$ is calculated by Eq. (3) at $T = 300$ K, but with the zero-temperature values of all dielectric permittivities. From Eq. (29) it is clear that $\Delta_T^{(1)} F_{\rm diff}$ represents the contribution to the thermal correction caused by a summation over the discrete Matsubara frequencies, whereas $\Delta_T^{(2)} F_{\rm diff}$ originates from the explicit dependence of dielectric permittivities on the temperature as a parameter.

At the end of this section, we briefly discuss the role of each of the two contributions to the thermal correction in the four theoretical models. If Au is described by the plasma model and free charge carriers in dielectrics are disregarded, it holds that

$$\Delta_T F^p_{\rm diff}(a,T) = \Delta_T^{(1)} F^p_{\rm diff}(a,T) > 0 \tag{30}$$

because in this case all dielectric permittivities are temperature independent.

If Au is described by the plasma model and free charge carriers in dielectrics are taken into account, we have

$$\begin{aligned} &\Delta_T^{(1)} F^{p,{\rm dc}}_{\rm diff}(a,T) = \Delta_T F^p_{\rm diff}(a,T), \\ &\Delta_T^{(2)} F^{p,{\rm dc}}_{\rm diff}(a,T) < 0. \end{aligned} \tag{31}$$

Note that the correction $\Delta_T^{(2)} F^{p,{\rm dc}}_{\rm diff}$ is given by the difference between the top dashed and the top solid lines in Fig. 5. For example, at separations of 0.5 and 1 μm $\Delta_T^{(2)} F^{p,{\rm dc}}_{\rm diff}$ is equal to –64.1 and –17.1 fN, respectively.

If Au is desctibed by the Drude model and the free charge carriers in dielectrics are disregarded, the dominant contribution to $\Delta_T F^D_{\rm diff}$ is given by

$$\Delta_T^{(1)} F^D_{\rm diff}(a,T) < 0. \tag{32}$$

The much smaller thermal correction $\Delta_T^{(2)} F^D_{\rm diff}$ originates from the difference in the values of the relaxation parameter of Au at $T = 0$ vs $T = 300$ K. As an example, one has $\Delta_T^{(1)} F^D_{\rm diff} = -207.0$ fN, $\Delta_T^{(2)} F^D_{\rm diff} = -7.0$ fN at $a = 0.5$ μm and $\Delta_T^{(1)} F^D_{\rm diff} = -58.0$ fN, $\Delta_T^{(2)} F^D_{\rm diff} = -0.8$ fN at $a = 1$ μm.

Finally, if Au is described by the Drude model and the free charge carriers in dielectrics are taken into account, one obtains

$$\begin{aligned} &\Delta_T^{(1)} F^{D,{\rm dc}}_{\rm diff}(a,T) = \Delta_T^{(1)} F^D_{\rm diff}(a,T), \\ &\Delta_T^{(2)} F^{p,{\rm dc}}_{\rm diff}(a,T) < 0. \end{aligned} \tag{33}$$

The latter correction contributes significantly to the total thermal correction. For example, at $a = 0.5$ and 1 μm $\Delta_T^{(2)} F^{D,{\rm dc}}_{\rm diff}$ is equal to –71.1 and –18.0 fN.

IV. EXPERIMENTAL TEST WITH AN ADDITIONAL SILICA LAYER

The experimental scheme discussed above (see Fig. 1) allows for good discrimination between the four theoretical approaches and for measurement of the thermal effect in the differential Casimir force. However, a practical drawback of this scheme is that it is not easy to produce the structured plate considered in this experiment. Specifically, even a small step between the plate sections made of high-resistivity Si and Au leads to considerable uncertainties in the theoretical predictions [50]. To avoid this problem and simultaneously

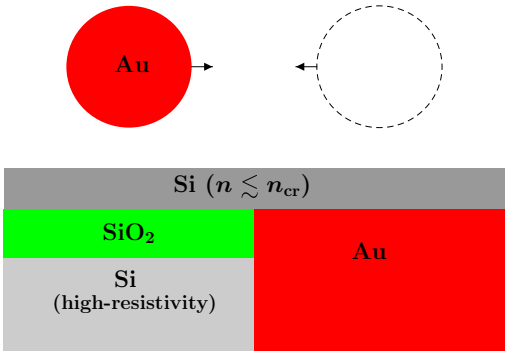

FIG. 6. The experimental configuration of a Au sphere moving back and forth above a structured plate with an additional SiO_2 layer. The P-doped Si overlayer is in the dielectric state. The measured quantity is the differential Casimir force $F_{\rm diff}$ between the Au sphere and the two halves of the plate when the sphere bottom is far away from their boundaries. The figure displays the two extreme positions of the sphere during its motion. The size of the sphere is not shown to scale.

increase the relative difference between the different theoretical predictions, we consider a slightly different experimental scheme. In the modified setup, the left section of the structured plate below the overlayer contains an additional layer made of SiO_2 (later denoted material 4) of thickness D followed by bulk high-resistivity Si (previously denoted material 3). The modified experimental scheme is shown in Fig. 6. An advantage of the modified structured plate is that it can be manufactured from a commercial wafer of Si grown on an insulator (SiO_2), i.e., a Si plate with a buried SiO_2 layer, following the procedure described in Refs. [2] and [32].

The Lifshitz-type formula, (3), for the differential Casimir force preserves its validity with the replacement

$$R_\alpha^{(0,2,3)}(i\zeta_l,y) \to R_\alpha^{(0,2,4,3)}(i\zeta_l,y), \tag{34}$$

where $R_\alpha^{(0,2,4,3)}(i\zeta_l,y)$ denotes the reflection coefficient of the modified left half of the plate in Fig. 6, which now consists of the Si overlayer, covering the plate sections made of SiO_2 and high-resistivity Si:

$$R_\alpha^{(0,2,4,3)}(i\zeta_l,y) = \frac{r_\alpha^{(0,2)}(i\zeta_l,y)+R_\alpha^{(2,4,3)}(i\zeta_l,y)e^{-d\sqrt{y^2+(\varepsilon_{2,l}-1)\zeta_l^2}/a}}{1+r_\alpha^{(0,2)}(i\zeta_l,y)R_\alpha^{(2,4,3)}(i\zeta_l,y)e^{-d\sqrt{y^2+(\varepsilon_{2,l}-1)\zeta_l^2}/a}}. \tag{35}$$

Here, the reflection coefficient $R_\alpha^{(2,4,3)}(i\zeta_l,y)$ of the SiO_2 and Si sections of the plate is given by

$$R_\alpha^{(2,4,3)}(i\zeta_l,y) = \frac{r_\alpha^{(2,4)}(i\zeta_l,y)+r_\alpha^{(4,3)}(i\zeta_l,y)e^{-D\sqrt{y^2+(\varepsilon_{4,l}-1)\zeta_l^2}/a}}{1+r_\alpha^{(2,4)}(i\zeta_l,y)r_\alpha^{(4,3)}(i\zeta_l,y)e^{-D\sqrt{y^2+(\varepsilon_{4,l}-1)\zeta_l^2}/a}}. \tag{36}$$

Note that the coefficients $r_\alpha^{(k,j)}$ are defined by Eq. (6) with the appropriately chosen upper indices.

Now we consider the behavior of the reflection coefficient, (35), at zero Matsubara frequency. It is easily seen that, irrespective of how one models the free charge carriers in the dielectric materials, it holds that

$$R_{\rm TE}^{(0,2,4,3)}(0,y)=0. \tag{37}$$

If the free charge carriers in the dielectric materials are taken into account, one obtains

$$R_{\rm TM}^{(0,2,4,3)}(0,y)=1. \tag{38}$$

The case of the TM reflection coefficient with free charge carriers in dielectric materials disregarded is the most interesting. In this case from Eq. (35) one arrives at

$$R_{\rm TM}^{(0,2,4,3)}(0,y) = \frac{r_{\rm TM,0}^{(0,2)}+R_{\rm TM}^{(2,4,2)}(0,y)e^{-dy/a}}{1+r_{\rm TM,0}^{(0,2)}R_{\rm TM}^{(2,4,2)}(0,y)e^{-dy/a}}, \tag{39}$$

where $r_{\rm TM,0}^{(0,2)}$ is defined in Eq. (15). The reflection coefficient $R_{\rm TM}^{(2,4,2)}(0,y)$ is given by

$$R_{\rm TM}^{(2,4,2)}(0,y) = r_{\rm TM,0}^{(2,4)}\frac{1-e^{-Dy/a}}{1-{r_{\rm TM,0}^{(2,4)}}^2e^{-Dy/a}}, \tag{40}$$

where

$$r_{\rm TM,0}^{(2,4)} = \frac{\varepsilon_{4,0}^{\rm cor}-\varepsilon_{2,0}^{\rm cor}}{\varepsilon_{4,0}^{\rm cor}+\varepsilon_{2,0}^{\rm cor}}, \tag{41}$$

and we have used the obvious identity

$$r_{\rm TM,0}^{(4,2)} = -r_{\rm TM,0}^{(2,4)}. \tag{42}$$

Numerical computations of the differential Casimir force were made using Eqs. (3) and (34)–(41). The dielectric permittivity of SiO_2 with disregarded free charge carriers, $\varepsilon_{4,l}^{\rm cor}$, is approximated to a high accuracy by the Ninham-Parsegian representation, which takes into account the effects of electronic and ionic polarization [60,61]. The oscillator parameters have been determined from a fit to optical data. The static dielectric permittivity of SiO_2 is $\varepsilon_{4,0}^{\rm cor}\approx 3.81$. Similarly to the case of high-resistivity Si, accounting for free charge carriers in SiO_2 affects the dielectric permittivity only at the zero Matsubara frequency and results in some dc conductivity. Taking into consideration that due to Eq. (37) the coefficient $R_{\rm TE}^{(0,2,4,3)}(0,y)$ does not depend on the inclusion or neglect of free charge carriers, their impact is determined by the coefficient $R_{\rm TM}^{(0,2,4,3)}(0,y)$ in accordance with Eqs. (38) and (39).

Computations have been performed at $T=300$ K taking the value of $d=200$ nm for the thickness of the P-doped overlayer and the value of $D=400$ nm for the thickness of the SiO_2 layer. The computational results for the differential Casimir force are presented in Fig. 7 as functions of the separation by the four lines, corresponding to the four theoretical approaches (the top pair of solid and dashed lines is computed using the plasma model for Au with free charge carriers in all dielectric materials disregarded and taken into account, respectively, whereas the bottom pair of lines is obtained using the Drude model for Au and the same options for free charges in dielectrics).

As shown in Fig. 7, all four theoretical approaches lead to widely distinct differential Casimir forces, which can be discriminated experimentally with certainty within the

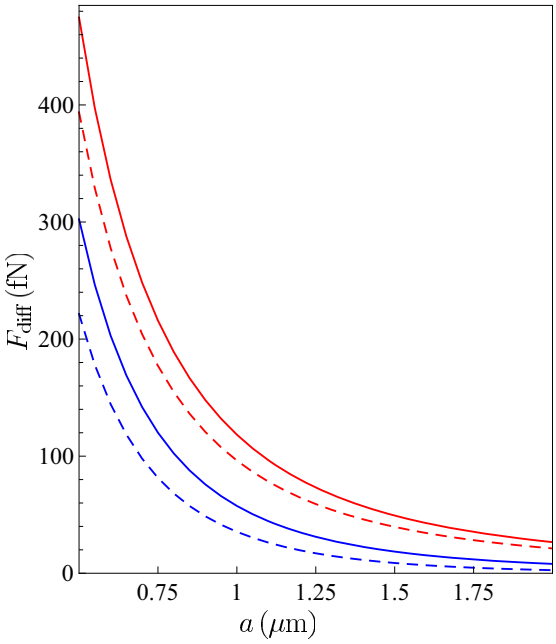

FIG. 7. Differential Casimir forces computed at $T = 300$ K in the configuration with an additional SiO_2 layer (Fig. 6) using the plasma model for Au with free charge carriers in dielectric materials disregarded and taken into account [top (red) pair of solid and dashed lines, respectively] and using the Drude model for Au with free charge carriers in dielectrics disregarded and included [bottom (blue) pair of solid and dashed lines, respectively] are shown as functions of the separation.

separation region from 0.5 to 2 μm. The computational results for the differential Casimir forces computed using the four theoretical approaches over the separation region from 0.5 to 3 μm are listed in Table I. The first column contains the separation value. The second and third columns list the values of $F^{p}_{\rm diff}$ and $F^{p,{\rm dc}}_{\rm diff}$ computed using the plasma model for Au with free charge carriers of dielectric materials disregarded and taken into account, respectively. The fourth and fifth columns present the values of $F^{D}_{\rm diff}$ and $F^{D,{\rm dc}}_{\rm diff}$ obtained using the Drude model for Au with free charge carriers of dielectric materials disregarded and taken into account, respectively.

According to Table I, at $a = 0.5$ μm the differences between the predicted values $F^{p}_{\rm diff}$ and $F^{p,{\rm dc}}_{\rm diff}$, between $F^{p,{\rm dc}}_{\rm diff}$ and $F^{D}_{\rm diff}$, and between $F^{D}_{\rm diff}$ and $F^{D,{\rm dc}}_{\rm diff}$ are equal to 80.22, 92.06, and 80.17 fN, respectively. At $a = 1.0$ and 1.6 μm the same differences are equal to 21.98, 38.86, and 21.98 and to 8.49, 19.06, and 8.48 fN, respectively. All these values are far in excess of the experimental sensitivity.

If the plasma model for Au is used in computations, the relative deviation of the differential Casimir force obtained with free charge carriers in dielectrics disregarded from that found with taken free charge carriers into account is

$$\delta F^{p}_{\rm diff} \equiv \frac{F^{p}_{\rm diff} - F^{p,{\rm dc}}_{\rm diff}}{F^{p,{\rm dc}}_{\rm diff}}. \tag{43}$$

From Table I one obtains that $\delta F^{p}_{\rm diff} = 20.3\%$, 22.8%, and 24.7% at separations $a = 0.5$, 1.0, and 1.6 μm, respectively. The analogous deviation between the next two theoretical approaches, defined as

$$\delta F^{p,{\rm dc};D}_{\rm diff} \equiv \frac{F^{p,{\rm dc}}_{\rm diff} - F^{D}_{\rm diff}}{F^{D}_{\rm diff}}, \tag{44}$$

is equal to 30.4%, 67.6%, and 124.4% at the same respective separations. Finally, the relative deviation of $F^{D}_{\rm diff}$ from $F^{D,{\rm dc}}_{\rm diff}$ is given by

$$\delta F^{D}_{\rm diff} \equiv \frac{F^{D}_{\rm diff} - F^{D,{\rm dc}}_{\rm diff}}{F^{D,{\rm dc}}_{\rm diff}}. \tag{45}$$

At separation distances $a = 0.5$, 1.0, and 1.6 μm one obtains from Table I $\delta F^{D}_{\rm diff} = 36.1\%$, 61.8%, and 124.0%, respectively. As for the relative deviation between the extreme two approaches, namely, the one which disregards both the relaxation properties of electrons in metals and the free charge carriers in dielectrics and the other which, instead, takes both into account, it is defined as

$$\delta F^{p;D,{\rm dc}}_{\rm diff} \equiv \frac{F^{p}_{\rm diff} - F^{D,{\rm dc}}_{\rm diff}}{F^{D,{\rm dc}}_{\rm diff}}. \tag{46}$$

From Table I one obtains that $\delta F^{p;D,{\rm dc}}_{\rm diff} = 113.6\%$, 233%, and 526.8% at the same respective separations. One can conclude that all the above relative deviations are sufficiently large for experimental discrimination between different theoretical approaches and all of them quickly increase with increasing separation.

We have also computed the thermal correction, (27), in the differential Casimir force in the configuration in Fig. 6 in the framework of the four theoretical approaches described above. The computational results at $T = 300$ K are shown in Fig. 8 as functions of the separation. The top pair of solid and dashed lines is obtained by using the plasma model for

TABLE I. Values of the differential Casimir force computed at $T = 300$ K in the configuration with an additional SiO_2 section using the plasma model for Au with free charge carriers in dielectric materials disregarded and taken into account (columns 2 and 3, respectively) and using the Drude model for Au with free charge carriers in dielectrics disregarded and included (columns 4 and 5, respectively) are listed at different separations (column 1).

a (μm)	$F^{p}_{\rm diff}$ (fN)	$F^{p,{\rm dc}}_{\rm diff}$ (fN)	$F^{D}_{\rm diff}$ (fN)	$F^{D,{\rm dc}}_{\rm diff}$ (fN)
0.5	474.57	394.35	302.29	222.12
0.6	336.31	278.28	202.96	144.96
0.7	248.13	204.43	141.86	98.18
0.8	189.07	155.13	102.39	68.46
0.9	147.94	120.90	75.88	48.86
1.0	118.36	96.38	57.52	35.54
1.2	80.00	64.72	34.94	19.67
1.4	57.27	46.10	22.56	11.40
1.6	42.87	34.38	15.32	6.84
1.8	33.26	26.61	10.86	4.21
2.0	26.56	21.22	7.98	2.64
2.2	21.72	17.34	6.07	1.68
2.4	18.11	14.46	4.74	1.09
2.6	15.36	12.26	3.80	0.71
2.8	13.20	10.55	3.12	0.46
3.0	11.48	9.19	2.61	0.31

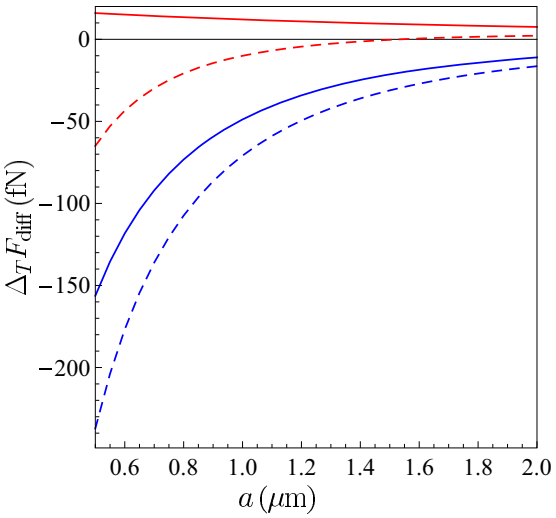

FIG. 8. Thermal corrections to the differential Casimir forces computed at $T = 300$ K in the configuration with an additional SiO_2 layer using the plasma model for Au with free charge carriers in dielectric materials disregarded and taken into account [top (red) pair of solid and dashed lines, respectively] and using the Drude model for Au with free charge carriers in dielectrics disregarded and included [bottom (blue) pair of solid and dashed lines, respectively] are shown as functions of the separation.

Au with free charge carriers in dielectrics disregarded and taken into account, respectively. The bottom pair of solid and dashed lines is computed by means of the Drude model for Au with respective neglect and inclusion of free charge carriers in dielectric materials. As can be seen in Fig. 8, over the separation range from 0.5 to 2 μm the thermal corrections predicted by the four theoretical approaches are significantly different and can be easily discriminated from each other taking into account the experimental sensitivity. Thus, at separations $a = 0.5$, 1.0, 1.5, and 2.0 μm the thermal correction using the plasma model with omitted conductivity of dielectrics, $\Delta_T F^{p}_{\rm diff}$, is equal to 16.0, 12.1, 9.4, and 7.6 fN, respectively. In a similar way, for the remaining three theoretical approaches one has

$$\begin{aligned}\Delta_T F^{p,\rm dc}_{\rm diff} &= -64.9,\ -10.0,\ -0.3,\ 2.2\ \text{fN},\\ \Delta_T F^{D}_{\rm diff} &= -156.3,\ -48.8,\ -21.4,\ -11.0\ \text{fN},\\ \Delta_T F^{D,\rm dc}_{\rm diff} &= -237.2,\ -70.8,\ -31.1,\ -16.4\ \text{fN}\end{aligned} \tag{47}$$

at the same respective separations.

V. ESTIMATION OF THEORETICAL ERRORS

Here, we present an estimation of errors inherent to the above computations. As mentioned in Sec. III, a conservative estimation of the minimum detectable force in experiments of this type is $\Delta F^{\rm expt}_{\rm diff} = 1$ fN. The total theoretical error in the determination of $F_{\rm diff}$ is contributed by several independent components and depends on the separation.

We begin with a possible error in the concentration of free charge carriers in the P-doped overlayer $\delta n = 5\%$ (see Fig. 6). This error does not influence the computed values of $F^{D}_{\rm diff}$ and $F^{p}_{\rm diff}$ when the free charge carriers in dielectric materials are disregarded but leads to the following errors if the free charge carriers are taken into account:

$$\begin{aligned}&\delta_n F^{D,\rm dc}_{\rm diff}(a_1) \approx 0.14\%, \quad \delta_n F^{D,\rm dc}_{\rm diff}(a_2) \approx 0.15\%,\\ &\delta_n F^{p,\rm dc}_{\rm diff}(a_1) \approx 0.08\%, \quad \delta_n F^{p,\rm dc}_{\rm diff}(a_2) \approx 0.02\%,\end{aligned} \tag{48}$$

where we present the values of errors at $a_1 = 0.5$ μm and $a_2 = 2$ μm. These results were obtained by repeating the computations in Sec. IV with $\tilde{n} = n \pm 0.05n$.

The second error source in theoretical values of the differential Casimir force is uncertainty in the thickness of the SiO_2 layer. For a commercial Si wafer $\Delta D = 2$ nm, leading to $\delta D = 0.5\%$ in our case. This leads to the following relative errors in our computational results:

$$\begin{aligned}&\delta_D F^{D}_{\rm diff}(a_1) \approx 0.05\%, \quad \delta_D F^{D}_{\rm diff}(a_2) \approx 0.075\%,\\ &\delta_D F^{p}_{\rm diff}(a_1) \approx 0.03\%, \quad \delta_D F^{p}_{\rm diff}(a_2) \approx 0.05\%,\\ &\delta_D F^{D,\rm dc}_{\rm diff}(a_1) \approx 0.04\%, \quad \delta_D F^{D,\rm dc}_{\rm diff}(a_2) \approx 0.06\%,\\ &\delta_D F^{p,\rm dc}_{\rm diff}(a_1) \approx 0.02\%, \quad \delta_D F^{p,\rm dc}_{\rm diff}(a_2) \approx 0.008\%.\end{aligned} \tag{49}$$

The third source of theoretical errors is the error in the thickness of the Si overlayer $\delta d = 2$ nm, i.e., $\delta d = 1\%$, resulting in

$$\begin{aligned}&\delta_d F^{D}_{\rm diff}(a_1) \approx 1.3\%, \quad \delta_d F^{D}_{\rm diff}(a_2) \approx 0.5\%,\\ &\delta_d F^{p}_{\rm diff}(a_1) \approx 1.05\%, \quad \delta_d F^{p}_{\rm diff}(a_2) \approx 0.5\%,\\ &\delta_d F^{D,\rm dc}_{\rm diff}(a_1) \approx 1.6\%, \quad \delta_d F^{D,\rm dc}_{\rm diff}(a_2) \approx 1.1\%,\\ &\delta_d F^{p,\rm dc}_{\rm diff}(a_1) \approx 1.1\%, \quad \delta_d F^{p,\rm dc}_{\rm diff}(a_2) \approx 0.3\%.\end{aligned} \tag{50}$$

All these errors are random quantities characterized by a uniform distribution. In this case the total relative error is obtained by a summation of the respective errors, (48)–(50) [2,62]:

$$\begin{aligned}&\delta_{\rm tot} F^{D}_{\rm diff}(a_1) \approx 1.4\%, \quad \delta_{\rm tot} F^{D}_{\rm diff}(a_2) \approx 0.6\%,\\ &\delta_{\rm tot} F^{p}_{\rm diff}(a_1) \approx 1.1\%, \quad \delta_{\rm tot} F^{p}_{\rm diff}(a_2) \approx 0.6\%,\\ &\delta_{\rm tot} F^{D,\rm dc}_{\rm diff}(a_1) \approx 1.8\%, \quad \delta_{\rm tot} F^{D,\rm dc}_{\rm diff}(a_2) \approx 1.3\%,\\ &\delta_{\rm tot} F^{p,\rm dc}_{\rm diff}(a_1) \approx 1.2\%, \quad \delta_{\rm tot} F^{p,\rm dc}_{\rm diff}(a_2) \approx 0.3\%,\end{aligned} \tag{51}$$

There is one more theoretical uncertainty originating from errors in the dielectric permittivities. At separations in the micrometer range, errors in the optical data do not lead to noticeable errors in the differential Casimir force. However, depending on the properties of a specific Au sample and its preparation process, the minimum possible value of the plasma frequency of Au was found to be $\omega^{\rm min}_{p,1} \approx 6.8$ eV [63,64]. The corresponding value of the relaxation parameter is $\gamma^{\rm min}_1 \approx 0.02$ eV. In fact, different values of $\omega_{p,1}$ in the interval from 6.8 to 9.0 eV cannot be considered as random values of the measured quantity because they correspond to different samples. It would be preferable to determine the value of ω_p for the specific sample used in measurements of the Casimir force as done in Refs. [22] and [23]. However, for illustrative purposes, here we present the relative deviations of the value of $F_{\rm diff}$ which would be obtained upon using for the plasma frequency the value $\omega^{\rm min}_{p,1}$ instead of the value $\omega_{p,1} = 9.0$ eV

that was used above:

$$\delta_{\omega_p} F^{D}_{\rm diff}(a_1) \approx -0.7\%, \quad \delta_{\omega_p} F^{D}_{\rm diff}(a_2) \approx -0.03\%,$$
$$\delta_{\omega_p} F^{p}_{\rm diff}(a_1) \approx -1.5\%, \quad \delta_{\omega_p} F^{p}_{\rm diff}(a_2) \approx -0.6\%,$$
$$\delta_{\omega_p} F^{D,{\rm dc}}_{\rm diff}(a_1) \approx -1.3\%, \quad \delta_{\omega_p} F^{D,{\rm dc}}_{\rm diff}(a_2) \approx -0.8\%,$$
$$\delta_{\omega_p} F^{p,{\rm dc}}_{\rm diff}(a_1) \approx -0.6\%, \quad \delta_{\omega_p} F^{p,{\rm dc}}_{\rm diff}(a_2) \approx -0.85\%. \quad (52)$$

Some other effects which may influence the value of the differential force are the surface roughness and electrostatic patches. However, as noted in Refs. [40,42,50,51,65], the effect of patches is strongly suppressed in the differential force, whereas the effect of roughness is negligible in the micrometer separation range [2,3,41]. Note that in comparisons between the measurement data and theory in the proposed experiment one should correct the theoretical values in Table I for deviations from the proximity force approximation used in Eq. (3). This correction can be estimated as about –0.2% of $F_{\rm diff}$ [24,53–55].

From Eqs. (51) and (52) it is seen that even taking into account all possible errors and uncertainties the theoretical predictions of the four approaches discussed above differ considerably and can be easily discriminated by performing the proposed experiment.

VI. DISCUSSION AND CONCLUSIONS

In the foregoing, we have suggested a universal setup allowing us to directly measure the thermal effect in the Casimir force and to determine the role of free charge carriers in both metallic and dielectric materials, in a single experiment. According to our results, these aims can be achieved by measuring the differential Casimir force between a Au-coated sphere moving back and forth above a structured plate covered with a conductive overlayer. One half of the plate is made of high-resistivity dielectric materials, while the other half is made of Au. The main novel feature of this setup is that the conductive overlayer is made of a doped semiconductor (P-doped Si in our case) whose concentration of free charge carriers is only slightly below the critical one, where the dielectric-to-metal phase transition occurs. Thus, the overlayer is made of a dielectric material possessing a rather high conductivity at room temperature, allowing for the electrostatic calibration required in precise measurements of the Casimir force.

We have considered two versions of the structured plate where the dielectric section is made either of bulk high-resistivity Si or of a layer of SiO_2 followed by bulk high-resistivity Si. In both cases the differential Casimir force was calculated over the separation region from 0.5 μm to a few micrometers, i.e., in the domain where thermal effects determined by the zero-frequency term in the Lifshitz formula contribute considerably.

Computations have been performed within the four theoretical approaches discussed in the literature, i.e., Au at low frequencies is described by the plasma model and the free charge carriers in all dielectric materials (including the P-doped Si) are either disregarded or taken into account or Au at low frequencies is described by the Drude model and the free charge carriers in all dielectric materials are again either disregarded or taken into account. We have also calculated the dependence of all differential forces on the thickness of the P-doped Si overlayer, determined the thermal contribution to the differential Casimir force at different separations, and estimated all related errors and uncertainties.

The obtained results allow us to conclude that all four theoretical approaches lead to significantly different values of the differential Casimir force in the micrometer separation range, which are many times larger than both the experimental and the theoretical errors. Thus, the proposed experiment is capable of providing an unequivocal confirmation of one of the above theoretical models and rule out the other three. Our calculation results show that the thermal effect in the differential Casimir force is up to two and one orders of magnitude larger than the minimum detectable signal when the Drude and plasma models are used, respectively. Because of this, the proposed experiment not only can lead to confirmation of one of the models, but also allows reliable measurement of the thermal contribution to the observed signal.

One may guess which of the four above theoretical approaches has the best chances of being confirmed. As discussed in Sec. I, previous experiments with metallic test bodies [20–26,43] are in agreement with the plasma model and exclude the Drude model, whereas only the experiment [28] leads to the opposite conclusion. Concurrently, several other experiments performed with dielectric test bodies [31–35] are in agreement with theory disregarding the free charge carriers and exclude theory taking the free charge carriers into account. On this basis, it is reasonable to expect that the proposed universal experiment may confirm the theoretical prediction $F^{p}_{\rm diff}$ obtained using the plasma model at low frequencies for Au with free charge carriers in dielectric materials disregarded. It should be emphasized, however, that almost all of the above-mentioned experiments (with the exception of only Refs. [28] and [31]) are most precise at separations below 0.5 μm and use quite distinct experimental setups. This allows us to conclude that the proposed universal experiment, which is capable of determining the role of free charge carriers in the Casimir force between any materials and measuring the thermal effect in the micrometer separation range, will bring challenging results for the theory of electromagnetic fluctuations.

ACKNOWLEDGMENTS

The work of V.M.M. was partially supported by the Russian Government Program of Competitive Growth of Kazan Federal University.

[1] H. B. G. Casimir, Proc. Kon. Ned. Akad. Wet. B **51**, 793 (1948).
[2] M. Bordag, G. L. Klimchitskaya, U. Mohideen, and V. M. Mostepanenko, *Advances in the Casimir Effect* (Oxford University Press, Oxford, UK, 2015).
[3] G. L. Klimchitskaya, U. Mohideen, and V. M. Mostepanenko, Rev. Mod. Phys. **81**, 1827 (2009).
[4] A. W. Rodrigues, F. Capasso, and S. G. Johnson, Nature Photon. **5**, 211 (2011).

[5] L. M. Woods, D. A. R. Dalvit, A. Tkatchenko, P. Rodrigues-Lopez, A. W. Rodrigues, and R. Podgornik, Rev. Mod. Phys. **88**, 045003 (2016).

[6] V. A. Parsegian, *Van der Waals Forces: A Handbook for Biologists, Chemists, Engineers, and Physicists* (Cambridge University Press, Cambridge, UK, 2005).

[7] E. M. Lifshitz, Zh. Eksp. Teor. Fiz. **29**, 94 (1955) [Sov. Phys. JETP **2**, 73 (1956)].

[8] M. Boström and Bo E. Sernelius, Phys. Rev. Lett. **84**, 4757 (2000).

[9] M. Bordag, B. Geyer, G. L. Klimchitskaya, and V. M. Mostepanenko, Phys. Rev. Lett. **85**, 503 (2000).

[10] V. B. Bezerra, G. L. Klimchitskaya, and V. M. Mostepanenko, Phys. Rev. A **65**, 052113 (2002).

[11] V. B. Bezerra, G. L. Klimchitskaya, and V. M. Mostepanenko, Phys. Rev. A **66**, 062112 (2002).

[12] V. B. Bezerra, G. L. Klimchitskaya, V. M. Mostepanenko, and C. Romero, Phys. Rev. A **69**, 022119 (2004).

[13] M. Bordag and I. G. Pirozhenko, Phys. Rev. D **82**, 125016 (2010).

[14] G. L. Klimchitskaya and C. C. Korikov, Phys. Rev. A **91**, 032119 (2015); **92**, 029902(E) (2015).

[15] P. R. Buenzli and P. A. Martin, Phys. Rev. E **77**, 011114 (2008).

[16] G. Bimonte, Phys. Rev. A **79**, 042107 (2009).

[17] G. Bimonte, New J. Phys. **9**, 281 (2007).

[18] F. Intravaia and C. Henkel, Phys. Rev. Lett. **103**, 130405 (2009).

[19] F. Intravaia, S. A. Ellingsen, and C. Henkel, Phys. Rev. A **82**, 032504 (2010).

[20] R. S. Decca, E. Fischbach, G. L. Klimchitskaya, D. E. Krause, D. López, and V. M. Mostepanenko, Phys. Rev. D **68**, 116003 (2003).

[21] R. S. Decca, D. López, E. Fischbach, G. L. Klimchitskaya, D. E. Krause, and V. M. Mostepanenko, Ann. Phys. (NY) **318**, 37 (2005).

[22] R. S. Decca, D. López, E. Fischbach, G. L. Klimchitskaya, D. E. Krause, and V. M. Mostepanenko, Phys. Rev. D **75**, 077101 (2007).

[23] R. S. Decca, D. López, E. Fischbach, G. L. Klimchitskaya, D. E. Krause, and V. M. Mostepanenko, Eur. Phys. J. C **51**, 963 (2007).

[24] C.-C. Chang, A. A. Banishev, R. Castillo-Garza, G. L. Klimchitskaya, V. M. Mostepanenko, and U. Mohideen, Phys. Rev. B **85**, 165443 (2012).

[25] A. A. Banishev, G. L. Klimchitskaya, V. M. Mostepanenko, and U. Mohideen, Phys. Rev. Lett. **110**, 137401 (2013).

[26] A. A. Banishev, G. L. Klimchitskaya, V. M. Mostepanenko, and U. Mohideen, Phys. Rev. B **88**, 155410 (2013).

[27] V. M. Mostepanenko, J. Phys. Condens. Matter **27**, 214013 (2015).

[28] A. O. Sushkov, W. J. Kim, D. A. R. Dalvit, and S. K. Lamoreaux, Nat. Phys. **7**, 230 (2011).

[29] V. B. Bezerra, G. L. Klimchitskaya, U. Mohideen, V. M. Mostepanenko, and C. Romero, Phys. Rev. B **83**, 075417 (2011).

[30] G. L. Klimchitskaya, M. Bordag, E. Fischbach, D. E. Krause, and V. M. Mostepanenko, Int. J. Mod. Phys. A **26**, 3918 (2011).

[31] J. M. Obrecht, R. J. Wild, M. Antezza, L. P. Pitaevskii, S. Stringari, and E. A. Cornell, Phys. Rev. Lett. **98**, 063201 (2007).

[32] F. Chen, G. L. Klimchitskaya, V. M. Mostepanenko, and U. Mohideen, Phys. Rev. B **76**, 035338 (2007).

[33] C.-C. Chang, A. A. Banishev, G. L. Klimchitskaya, V. M. Mostepanenko, and U. Mohideen, Phys. Rev. Lett. **107**, 090403 (2011).

[34] A. A. Banishev, C.-C. Chang, R. Castillo-Garza, G. L. Klimchitskaya, V. M. Mostepanenko, and U. Mohideen, Phys. Rev. B **85**, 045436 (2012).

[35] G. L. Klimchitskaya and V. M. Mostepanenko, J. Phys. A **41**, 312002 (2008).

[36] B. Geyer, G. L. Klimchitskaya, and V. M. Mostepanenko, Phys. Rev. D **72**, 085009 (2005).

[37] G. L. Klimchitskaya, U. Mohideen, and V. M. Mostepanenko, J. Phys. A **41**, 432001 (2008).

[38] B. Geyer, G. L. Klimchitskaya, and V. M. Mostepanenko, Ann. Phys. (NY) **323**, 291 (2008).

[39] G. L. Klimchitskaya and C. C. Korikov, J. Phys. Condens. Matter **27**, 214007 (2015).

[40] R. O. Behunin, D. A. R. Dalvit, R. S. Decca, C. Genet, I. W. Jung, A. Lambrecht, A. Liscio, D. López, S. Reynaud, G. Schnoering, G. Voisin, and Y. Zeng, Phys. Rev. A **90**, 062115 (2014).

[41] P. J. van Zwol, G. Palasantzas, and J. Th. M. De Hosson, Phys. Rev. B **77**, 075412 (2008).

[42] G. Bimonte, Phys. Rev. Lett. **112**, 240401 (2014).

[43] G. Bimonte, D. López, and R. S. Decca, Phys. Rev. B **93**, 184434 (2016).

[44] R. S. Decca, D. López, H. B. Chan, E. Fischbach, D. E. Krause, and C. R. Jamell, Phys. Rev. Lett. **94**, 240401 (2005).

[45] Y.-J. Chen, W. K. Tham, D. E. Krause, D. López, E. Fischbach, and R. S. Decca, Phys. Rev. Lett. **116**, 221102 (2016).

[46] G. L. Klimchitskaya and V. M. Mostepanenko, Phys. Rev. A **92**, 042109 (2015).

[47] G. L. Klimchitskaya and V. M. Mostepanenko, Phys. Rev. A **93**, 042508 (2016).

[48] G. L. Klimchitskaya and V. M. Mostepanenko, Phys. Rev. B **94**, 045404 (2016).

[49] G. L. Klimchitskaya and V. M. Mostepanenko, Phys. Rev. A **95**, 012130 (2017).

[50] G. Bimonte, Phys. Rev. Lett. **113**, 240405 (2014).

[51] G. Bimonte, Phys. Rev. B **91**, 205443 (2015).

[52] T. F. Rosenbaum, R. F. Milligan, M. A. Paalanen, G. A. Thomas, R. N. Bhatt, and W. Lin, Phys. Rev. B **27**, 7509 (1983).

[53] G. Bimonte, T. Emig, R. L. Jaffe, and M. Kardar, Europhys. Lett. **97**, 50001 (2012).

[54] G. Bimonte, T. Emig, and M. Kardar, Appl. Phys. Lett. **100**, 074110 (2012).

[55] L. P. Teo, Phys. Rev. D **88**, 045019 (2013).

[56] Edited by E. D. Palik, *Handbook of Optical Constants of Solids* (Academic Press, New York, 1985).

[57] Edited by E. D. Palik, *Handbook of Optical Constants of Solids, Vol. 2* (Academic Press, New York, 1991).

[58] Edited by W. E. Beadle, J. C. C. Tsai, and R. D. Plummer, *Quick Reference Manual for Silicon Integrated Circuit Technology* (Wiley, New York, 1985).

[59] N. W. Ashcroft and N. D. Mermin, *Solid State Physics* (Saunders College, Philadelphia, 1976).

[60] D. B. Hough and L. R. White, Adv. Colloid Interface Sci. **14**, 3 (1980).

[61] L. Bergström, Adv. Colloid Interface Sci. **70**, 125 (1997).
[62] S. G. Rabinovich, *Measurement Errors and Uncertainties. Theory and Practice* (Springer, New York, 2000).
[63] V. B. Svetovoy, P. J. van Zwol, G. Palasantzas, and J. Th. M. De Hosson, Phys. Rev. B **77**, 035439 (2008).
[64] P. J. van Zwol, G. Palasantzas, M. van de Schootbrugge, and J. Th. M. De Hosson, Appl. Phys. Lett. **92**, 054101 (2008).
[65] R. O. Behunin, D. A. R. Dalvit, R. S. Decca, and C. C. Speake, Phys. Rev. D **89**, 051301(R) (2014).